An upgraded G-band differential absorption radar system for future airborne studies

Richard J. Roy, Ken B. Cooper, Matthew Lebsock, Luis Millán, Jose Siles, Robert Dengler, and Raquel Monje
Jet Propulsion Laboratory, California Institute of Technology
Pasadena, CA, USA

***Abstract*—A proof-of-concept, 170 GHz frequency-modulated, continuous-wave (FMCW) radar has been developed for measuring water vapor profiles within the cloudy boundary layer from an airborne platform. The measurement concept exploits the differential absorption accrued by two or more transmitted frequencies in the vicinity of the 183 GHz water absorption line to retrieve range-resolved humidity profiles, so-called differential absorption radar (DAR). The upgraded system design includes important considerations for monostatic radar operation with an open fuselage viewport (i.e. no radome). The radar features an all-solid-state tansmitter with > 0.4 W continuous transmit power, a 60 cm primary aperture and corresponding 58 dB antenna gain, and more than 80 dB transmit/receive isolation, enabling near thermal-noise-limited sensitivity with a 8 dB noise-figure receiver. Ice-cloud radar returns are detected beyond 8 km in height from the ground, demonstrating the high sensitivity of the system. In addition to in-cloud humidity profiling capabilities, deployment of a water vapor DAR from an airborne platform enables measurements of total column water vapor (TCWV) for all weather and surface scenarios. Precision estimates and potential biases for future TCWV measurements are discussed.**

***Index Terms*—millimeter-wave radar, FMCW, differential absorption radar, humidity sounding**

I. Introduction

The water absorption line centered at 183 GHz is utilized by many passive remote sensing platforms to perform atmospheric humidity sounding, including the advanced microwave sounding units (AMSUs) and the humidity sounder for Brazil (HSB). However, these systems, as well as passive infrared sounders and GNSS radio occultation techniques, have limited ability to perform high-resolution observations of vertical water vapor profiles in the presence of clouds, contributing to deficiencies in numerical weather and climate change prediction capabilities [1], [2]. To fill this observational gap, we are currently developing a proof-of-concept FMCW radar instrument at 170 GHz to perform differential absorption radar (DAR) measurements from an airborne platform. This work leverages FMCW radar technology previously demonstrated at the Jet Propulsion Laboratory (JPL) at 675 GHz for security imaging, and at 94 GHz for compact planetary/comet Doppler radar applications [3], [4]. State-of-the-art components designed at JPL that maximize the radar sensitivity include high output power G-band frequency multipliers and InP low-noise amplifiers.

By using a frequency-tunable transmitter that scans a flank of the 183 GHz absorption line, we can compare the relative absorption at different frequencies from in-cloud and surface radar echoes to retrieve in-cloud humidity profiles and total column water vapor, respectively. In recent work, we have demonstrated the water vapor DAR technique from a ground platform using an FMCW radar operating between 167 and 174.8 GHz, and implemented retrieval algorithms to obtain humidity profiles within clouds and precipitation with 200 m resolution [5], [6]. The radar's transmission band is restricted to operate at these frequencies due to allocation of various bands near the 183 GHz water line for passive sensors [7]. These initial tests were performed using a transmitter featuring 140 mW transmit power and 39 dB antenna gain, and a receiver that shares the same quasi-optical path as the transmitter. Typically, monostatic FMCW radar operation results in degraded sensitivity due to spectrally broad transmitter phase noise that accompanies target echos, often with the strongest effect coming from unintended reflections near zero range. However, for this 170 GHz FMCW radar, thermal-noise-limited sensitivity is achieved using a quasi-optical, polarization-based duplexing technique that provides more than 80 dB of isolation (for more details see [8]).

In this work, we present an updated design for the 170 GHz system, including a transmitter with 58 dB antenna gain and more than 400 mW transmit power across the entire transmission band, which is a record high efficiency ($\approx 25\%$) for such high power using solid-state sources at these frequencies. In preliminary ground-based tests with the new system, ice-cloud returns beyond 8 km in height are detected, highlighting the radar's high sensitivity despite large atmospheric attenuation within the boundary layer. The instrument, dubbed the vapor in-cloud profiling radar, or VIPR, will be deployed in the near future from an airborne platform as a proof-of-concept for potential future spaceborne DAR measurements of water vapor inside of clouds. Furthermore, when deployed on an aircraft, the 170 GHz radar will collect radar returns from the Earth's surface regardless of cloud cover, which can be used to retrieve total column water vapor (TCWV). In fact, such an application of DAR is a promising avenue towards spaceborne deployment, as the necessary sensitivity is considerably less than that needed for in-cloud humidity profiling from space because of the large difference in backscattering cross section. An important advantage of DAR measurements of TCWV over existing passive methods in the visible, infrared, and microwave regions is the ability to perform the measurement for all surface types, at all times of day, and in the presence (or absence) of clouds, whereas the passive methods each suffer

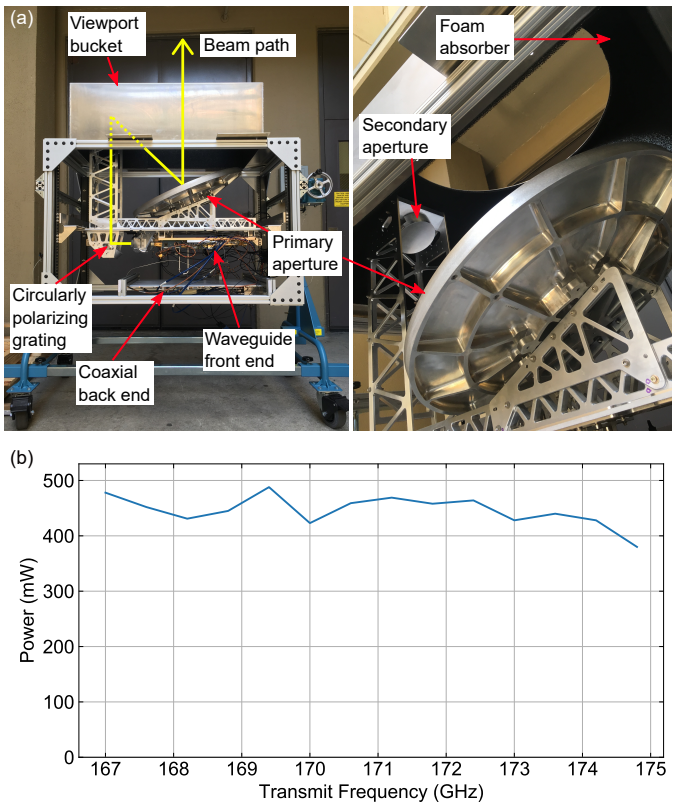

Fig. 1. (a) Photo of the VIPR system for ground-based testing, with 60 cm viewport bucket to mimic aircraft fuselage. To minimize T/R leakage from stray beam energy, the bucket is coated with foam absorber. (b) Transmit power across the DAR band.

from one or more of these sampling problems. Here we provide a brief discussion of uncertainty and bias considerations for a TCWV measurement from an aircraft.

II. Airborne DAR Design

Since using a radome would likely reduce transmit/receive (T/R) isolation, leading to signal-to-noise degradation, an airborne version of VIPR should operate with an open viewport. However, even with clear path for the radar beam to exit, it is important to consider the potential degradation of the T/R isolation within the fuselage from aperture spillover and low-level side lobes. In order to investigate these effects, we utilize an artificial 60 cm diameter viewport as shown in figure 1(a), where an aluminum sheet metal "bucket" is mounted on a Flotron rotation fixture to permit zenith pointing capability. As part of the quasi-optical T/R duplexing method, the orthogonal linear polarization modes of the transmit and receive feeds undergo a transformation to oppositely circular polarization upon diffracting off of a reflector grating (see figure 1(a)). Importantly, any beam reflections that occur after the transmitted beam becomes circularly polarized couple directly into the receiver, making it critical to minimize the amount of beam energy that does not exit the viewport. Figure 1(b) shows the transmitter output power, with an average of 450 mW across the transmit band. Such a high output

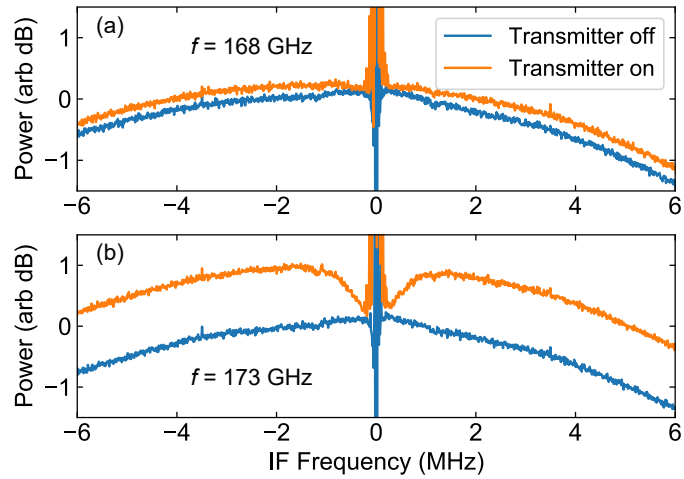

Fig. 2. Effects of transmitter phase noise with a -30 dB taper and with the viewport bucket installed (with absorber). (a) Best case and (b) worst case scenarios within the 167 to 174.8 GHz band are shown.

power for an all solid-state transmitter at G-band is achieved using GaN MMIC W-band amplifiers to pump multiple GaAs Schottky diode frequency multipliers, the outputs of which are subsequently power-combined in a compact waveguide block. For more information see [9].

Because of T/R leakage considerations, two optics designs were attempted featuring featuring tapers on the primary aperture of -12 and -30 dB, with corresponding gains of 60 and 58 dB, estimated using physical optics simulations. In preliminary tests without the viewport bucket, operating with the more aggressive -12 dB taper resulted in a significant increase in the background noise floor, likely from direct leakage of primary aperture spillover into the receiver, while the -30 dB taper maintains a very high level of T/R isolation. Thus, in the current system, it is necessary to sacrifice the additional 2 dB of antenna gain and implement the -30 dB taper to minimize the amount of stray beam energy within the bucket. Furthermore, in order to guard against internal reflections coupling into the receiver, we coat the entire interior surface of the bucket with 1/4″ RFRET foam absorber from Laird Technologies. The resulting phase noise effects from T/R leakage with the bucket installed are shown in figure 2, where we show the radar IF spectrum with the transmitter on and off for two different frequencies exemplifying the best and worst performance across the 167 to 174.8 GHz band. The variable behavior across the transmission band is likely due to free-space standing waves between the receiver and dominant reflection points. Though not shown in the figure, without the absorber present the noise floor rises by more than 10 dB due to transmitter phase noise. Furthermore, we note that with the transmitter on the IF spectrum looks identical with or without the bucket present, signifying that the absorber completely mitigates deleterious effects from bucket reflections.

The range of phase noise levels in figure 2 are 0.2 to 1 dB above the thermal noise floor, corresponding to a phase noise power of 5% to 25% of the thermal noise power. In general,

TABLE I
UPGRADED RADAR SYSTEM PARAMETERS.

Parameter	Value	Unit
Transmit frequency	167 - 174.8	GHz
Transmit power	450	mW
Noise figure	< 8	dB
Primary aperture diameter	60	cm
Antenna gain	58	dB
Far-field beam width (FWHM)	0.26	degrees
Chrip bandwidth	60	MHz
Range resolution	2.5	m
Chirp time	1	ms

the point at which phase noise power equals thermal noise power signifies a state in which increasing the transmit power does not increase the radar sensitivity, since the noise floor will increase by roughly the same factor. Thus, the current system is not phase-noise limited for any transmit frequency, with much of the transmit band featuring thermal-noise-limited performance. Important system parameters are collected in table I, where the noise figure reported is for a complex radar signal detected using a double-sideband front-end mixer.

III. Ground Testing with Artificial Viewport

For initial testing of VIPR with the viewport bucket installed, it has been deployed from the ground in the zenith-pointing configuration for two different weather scenarios. For these tests, the radar parameters and signal processing procedures are identical to those used in [6]. Briefly, a chirp bandwidth of 60 MHz results in a nominal range resolution of 2.5 m. After acquiring N_p pulses of 1 ms duration at each transmit frequency, the resulting spectra are averaged, and downsampled to a final range resolution of 27.5 m, in order to beat down statistical uncertainty from radar speckle. To estimate the contribution to the total signal power coming from target echos, it is necessary to subtract off the background noise floor at each point in the IF spectrum. This noise floor is continuously measured throughout the cloud measurement by employing a triangle-wave chirp waveform, which switches the position of the cloud signal from positive to negative IF frequency depending on the FM slope. Thus, by suitably subtracting the average spectra from positively and negatively sloped chirps, the cloud echo power spectrum $P_e(r)$ is obtained.

Figure 3 shows echo power spectra for two different cloud scenarios, where the power at each range is scaled by the r^2, and the individual traces are normalized to their value at some near range. The spreading of the different frequencies after this normalization point due to differential absorption from water vapor, and can be used to extract range resolved maps of humidity. Figure 3(a) shows measurements of near surface cloud/fog, which is composed of very small liquid droplets and thus is a weak signal. The profile in figure 3(b) was measured during a pre-frontal event, and displays two distinct cloud layers separated by roughly 3 km. For the lowest two frequencies, returns from ice cloud particles out to 8 km are observed, highlighting the high sensitivity of the system.

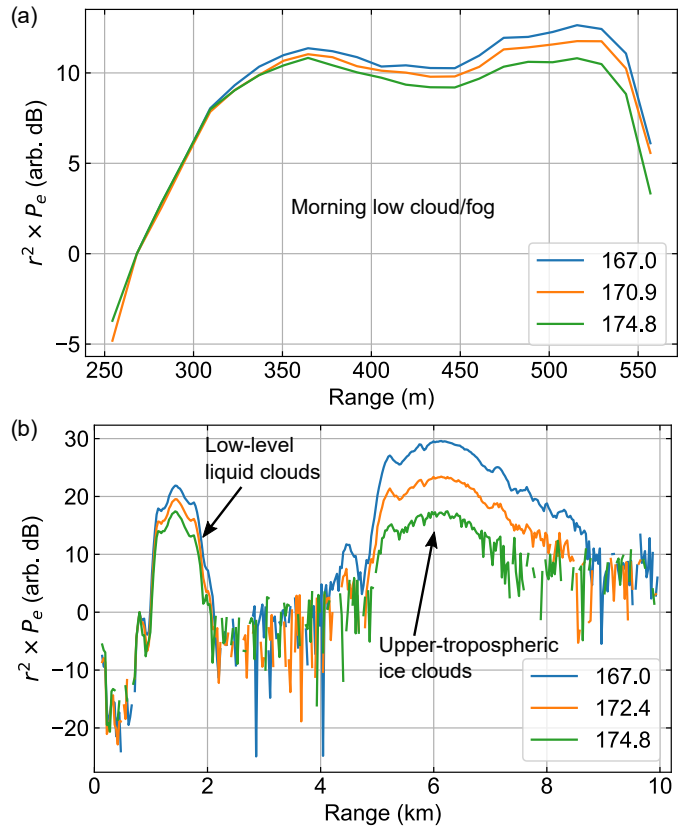

Fig. 3. Ground-based testing (zenith-pointing) of VIPR with the viewport bucket. (a) Measurements of near-surface cloud/fog. (b) Multiple cloud layers, with ice-cloud detection beyond 8 km. Note the different scales for the range axes.

These measurements show that the system will be effective at sampling cloudy volumes in the lower troposphere while flying at an altitude of 4 to 5 km, since the radar beam clearly penetrates well beyond this height from a ground platform.

In coming months, radar calibration measurements using metal spheres will be performed, allowing for absolute calibration of the echo power spectra in units of dBZ. With these absolutely calibrated returns, we can extend the retrieval analysis detailed in [6] to include retrieval of liquid/ice properties of clouds. Furthermore, it is required to know the relative gain factors at two or more frequencies in order to perform the total column water vapor retrieval, as we'll briefly discuss in the next section.

IV. TCWV Bias and Precision Estimates

There are two important advantages to deploying the DAR from an airborne platform as opposed to from the ground: (1) the motion of the aircraft allows for vastly increased spatial sampling, and (2) the returns from the Earth's surface permit a measurement of TCWV regardless of cloud cover. In general, the power received at the radar from the surface echo is given by [10]

$$P_e(r_s, f) = C(f)\sigma_0(f)r_s^{-2}\exp(-2\tau(r_s, f)), \qquad (1)$$

where $C(f) = P_t(f)G_{\text{rec}}(f)G_a^2(f)\Omega c^2/((4\pi)^3 f^2)$, P_t is the transmit power, G_{rec} is the receiver gain, G_a is the antenna gain, Ω is the two-way solid angle, c is the speed of light, σ_0 is the normalized surface cross section, r_s is the distance to the surface, and

$$\tau(r_s, f) = \int_0^{r_s} dr(\beta_{\text{gas}}(r, f) + \beta_{\text{part}}(r, f)) \tag{2}$$

is the one-way optical depth. Here β_{gas} and β_{part} are the gaseous and particulate extinction coefficients, respectively. In the viscinity of the 183 GHz water line, we can replace $\beta(r, f) = \kappa_v(r, f)\rho_v(r)$, where $\kappa_v(r, f)$ is the mass extinction cross section for water vapor, and ρ_v is the water vapor density.

Assuming that κ_v does not vary much between the aircraft and the surface, one can find a simple expression for the TCWV using surface echo measurements at two frequencies f_1 and f_2,

$$\begin{aligned}\text{TCWV} &= \int_0^{r_s} dr\rho_v(r) \\ &= \frac{1}{2\Delta\kappa_v}\left[\ln\left(\frac{P_e(r_s, f_1)}{P_e(r_s, f_2)}\right) + \ln\left(\frac{C(f_2)}{C(f_1)}\right)\right. \\ &\quad \left. + \ln\left(\frac{\sigma_0(f_2)}{\sigma_0(f_1)}\right) - 2\int_0^{r_s} dr\Delta\beta_{\text{part}}(r)\right], \end{aligned} \tag{3}$$

where $\Delta\kappa_v = \kappa_v(f_2) - \kappa_v(f_1)$ and similarly for $\Delta\beta_{\text{part}}$. For the purposes of error analysis, we consider the terms on the right hand side of equation (3) one at a time, and write $\ln(\cdots) = \ln(\alpha)$ for the three ratio terms. Then, using standard error propagation we find

$$\frac{\sigma_{\text{TCWV}}}{\text{TCWV}} = \frac{1}{2\Delta\tau}\frac{\sigma_\alpha}{\alpha}. \tag{4}$$

For typical atmospheric conditions with $f_1 = 167$ GHz and $f_2 = 174.8$ GHz, $\Delta\kappa_v \approx 0.26$ dB/km/(g/m^3), and using a mean humidity in the lowest 5 km of 5 g/m^3, we find $\Delta\tau = \Delta\kappa_v\rho_v r_s = 1.5$. Thus, an uncertainty of 10% in any of the ratios in equation (3) translates to a TCWV error of 3.3%.

An important potential source of TCWV bias is the differential particulate extinction term in equation (3). Practically, if a measurement contains a cloud signal at any height, it does not make sense to use the surface return to perform a total column measurement, since the presence of the cloud echos allows for splitting the atmosphere into multiple levels for the humidity retrieval, which is always preferred. Therefore, situations where the differential particulate scattering biases are important for column measurements are those where cloud particle sizes are small enough, or the cloud is far enough from the radar, that the cloud reflectivity is below the sensitivity of the system. In this case the integration of the particulate extinction through the cloud becomes an unknowable bias. This may occur for low marine stratocumulus in airborne studies. Treating the hydrometeor scattering in the Rayleigh limit, we calculate the differential particulate extinction from $\Delta\beta_{\text{part}} = 6\pi\,\text{LWC}\,\text{Im}(K_w)(f_2 - f_1)/(\rho_w c)$, where LWC is the liquid water content, K_w is the frequency dependent dielectric factor for liquid water, and ρ_w is the density of liquid water [11]. Using LWC $= 0.1$ g/m^3 and the same values for f_1 and f_2, we find $\Delta\beta_{\text{part}} = 0.04$ dB/km. Therefore, assuming that the low cloud spans the lowest 2 km of the atmosphere, we find that this results in a TCWV bias of 1%. From this analysis it is clear that low marine stratocumulus should not prevent accurate measurements of TCWV from an airborne platform.

V. Conclusion

We have presented an upgraded version of the JPL VIPR instrument, with the ability to both profile water vapor inside of clouds and measure TCWV in clear sky areas if deployed from an aircraft. The system features state-of-the-art solid-state components enabling record high transmit powers at 170 GHz. The sensitivity of the radar is highlighted by detection of ice clouds beyond 8 km in range. In coming months, the radar transceiver will be calibrated using a target with known cross section, enabling column water vapor measurements and retrieval of cloud liquid/ice particle properties. Furthermore, validation measurements with coincident radiosonde launches are planned for the near future. Subsequently, the system will be deployed from an airborne platform, and the water vapor measurements demonstrated over various cloud scenes and surface types.

Acknowledgment

This research was supported by NASA's Earth Science Technology Office under the Instrument Incubator Program, and was carried out at the Jet Propulsion Laboratory (JPL), California Institute of Technology, Pasadena, CA, USA, under contract with the National Aeronautics and Space Administration. R. Roy's research was supported by an appointment to the NASA Postdoctoral Program at JPL, administered by Universities Space Research Association under contract with NASA. Copyright 2018 California Institute of Technology. U.S. Government sponsorship acknowledged.

References

[1] S. A. Buehler, M. Kuvatov, T. R. Sreerekha, V. O. John, B. Rydberg, P. Eriksson, and J. Notholt, "A cloud filtering method for microwave upper tropospheric humidity measurements," *Atmospheric Chemistry and Physics*, vol. 7, no. 21, pp. 5531–5542, 2007.

[2] T. J. Greenwald and S. A. Christopher, "Effect of cold clouds on satellite measurements near 183 ghz," *Journal of Geophysical Research: Atmospheres*, vol. 107, no. D13, pp. AAC 3–1–AAC 3–8, 2002.

[3] K. B. Cooper, R. J. Dengler, N. Llombart, B. Thomas, G. Chattopadhyay, and P. H. Siegel, "Thz imaging radar for standoff personnel screening," *IEEE Transactions on Terahertz Science and Technology*, vol. 1, no. 1, pp. 169–182, Sept 2011.

[4] K. B. Cooper, R. R. Monje, M. Alonso-delPino, R. J. Dengler, C. J. Cochrane, S. L. Durden, A. Tang, and M. Choukroun, "A w-band comet-jet doppler radar prototype," in *2018 IEEE Radar Conference (RadarConf18)*, 2018, pp. 0202–0205.

[5] K. B. Cooper, R. R. Monje, L. Millán, M. Lebsock, S. Tanelli, J. V. Siles, C. Lee, and A. Brown, "Atmospheric humidity sounding using differential absorption radar near 183 ghz," *IEEE Geoscience and Remote Sensing Letters*, vol. 15, no. 2, pp. 163–167, Feb 2018.

[6] R. J. Roy, M. Lebsock, L. Millán, R. Dengler, R. Rodriguez Monje, J. V. Siles, and K. B. Cooper, "Boundary-layer water vapor profiling using differential absorption radar," *Atmospheric Measurement Techniques Discussions*, vol. 2018, pp. 1–18, 2018.

[7] *Manual of Regulations and Procedures for Federal Radio Frequency Management*, from the National Telecommunications & Information Administration (NTIA), Revision of the May 2013 Edition, 2015.

[8] K. B. Cooper, N. Llombart, G. Chattopadhyay, B. Dengler, R. E. Cofield, C. Lee, S. Filchenkov, and E. Koposova, "A grating-based circular polarization duplexer for submillimeter-wave transceivers," *IEEE Microwave and Wireless Components Letters*, vol. 22, no. 3, pp. 108–110, March 2012.

[9] J. V. Siles, K. B. Cooper, C. Lee, R. Lin, G. Chattopadhyay, and I. Mehdi, "A new generation of room-temperature frequency multiplied sources with up to 10x higher output power in the 160 ghz - 1.6 thz range," *IEEE Transactions on Terahertz Science and Technology*, pp. 1–1, 2018.

[10] S. Tanelli, S. L. Durden, E. Im, K. S. Pak, D. G. Reinke, P. Partain, J. M. Haynes, and R. T. Marchand, "Cloudsat's cloud profiling radar after two years in orbit: Performance, calibration, and processing," *IEEE Transactions on Geoscience and Remote Sensing*, vol. 46, no. 11, pp. 3560–3573, 2008.

[11] R. Doviak and D. Zrnic, *Doppler Radar and Weather Observations (Second Edition)*. Mineola, NY: Dover Publications, Inc., 1993.